Harnessing Compositional Gradients to Elucidate Phase Behaviors Towards High Performance Polymer Semiconductor Blends

Rahul Venkatesh,[‡] Aaron L. Liu,[‡] Yulong Zheng,[†] Haoqun Zhao,[‡] Martha A. Grover,[‡,*] J. Carson Meredith[‡,*], and Elsa Reichmanis[¶,*]

[‡]*School of Chemical and Biomolecular Engineering, Georgia Institute of Technology, 311 Ferst Drive NW, Atlanta GA 30332, United States*

[†]*School of Chemistry and Biochemistry, Georgia Institute of Technology, 901 Atlantic Drive, Atlanta GA 30332, United States*

[¶]*Department of Chemical & Biomolecular Engineering, Lehigh University, 124 E. Morton Street, Bethlehem PA 18015, United States*

E-mail: elr420@lehigh.edu; martha.grover@chbe.gatech.edu; carson.meredith@chbe.gatech.edu

Abstract

Polymer semiconductor/insulator blends offer a promising avenue to achieve desired mechanical properties, environmental stability, and high device performance in organic field-effect transistors. A comprehensive understanding of process-structure-property relationships necessitates a thorough exploration of the composition space to identify transitions in performance, morphology, and phase behavior. Hence, this study employs a high-throughput gradient thin film library, enabling rapid and continuous screening of composition-morphology-device performance relationships in conjugated polymer blends. Applied to a donor-acceptor copolymer blend, this technique efficiently surveys a broad composition range, capturing trends in device performance across the gradient. Furthermore, characterizing the gradient library using microscopy and depth profiling techniques pinpointed composition-dependent transitions in morphology. To validate the results and gain deeper insights, uniform-composition experiments were conducted on select compositions within and outside the gradient range. Depth profiling experiments on the constant composition films unveil the presence of the semiconducting polymer at the air interface, with apparent enrichment of the semiconductor at the substrate interface at low ratios of the semiconducting component, transitioning to a more even distribution within the bulk of the film at higher ratios. The generalizability of the gradient approach was further confirmed by its application to a homopolymer under different solution processing conditions.

Key Words : Conjugated polymer-insulating polymer blends, High-throughput fabrication, Diketopyrrolopyrrole (DPP), Gradient film, donor-acceptor polymer, organic field effect transistor, phase separation.

Introduction

Polymer semiconductor/insulator blends (PSIBs) offer opportunities to induce thin film morphological motifs that provide improved electronic, environmental and mechanical performance in resultant devices, such as organic field effect transistors (OFETs) that utilize a conjugated polymer as the active layer.[1-7] Incorporating an insulating polymer such as polystyrene (PS) or polydimethylsiloxane (PDMS) has been shown to induce formation of a connected or 'networked' semiconducting polymer structure with improved charge transport characteristics.[1, 8-14] Even blend compositions with low weight fractions of the semiconducting component can achieve charge-carrier mobilities that match or even exceed those of devices made with only the semiconducting component.[1, 8, 12, 13] Notably, blend systems may also offer cost advantages due to reduced semiconductor source material requirements.[15] Additionally, PSIBs can enhance the air stability of OFETs making them more robust for practical applications.[13, 16] Furthermore, these blends can increase the biodegradability and stretchability of these devices, which are critical properties for emerging applications in flexible and wearable electronics.[13, 17] This combination of factors makes PSIBs a versatile and economically attractive option for advancing the performance and sustainability of organic electronic devices. Contingent upon the experimental conditions, phase separation between the organic semiconductor and insulating polymer within the blends can significantly influence final film morphology and device performance.[3, 11, 15, 18-20] In PSIBs, reported phase separation characteristics are diverse, ranging from vertical phase separation to apparently uniform material dispersion.[3, 6] Such variations depend on polymer intrinsic characteristics (e.g., chemical structure, molecular weight, solubility, substrate interactions) and the deposition conditions.[3, 6, 21, 22]

Despite the substantial promise of PSIBs, significant knowledge gaps persist in understanding the process-structure-property relationships (PSPR). Phase transitions and morphological changes that are critical to understanding the performance of PSIBs can occur within narrow composition windows, which could be overlooked if the entire composition space is not comprehensively examined under the same deposition conditions. Moreover, the complexity escalates when exploring composition-performance trends with respect to different polymers/solvents or incorporation of additional solution processing steps (e.g. UV-irradiation,[1] ultrasonication,[23] aging[4]). Identifying the blend composition where improved device performance

is first achieved with minimal semiconductor content can be challenging and costly. To optimize the performance of PSIBs, a comprehensive understanding of the intricate composition-performance relationship governing PSIB behavior is needed.

High-throughput experimentation (HTE) has emerged as an effective approach to address the lack of sufficient data for materials optimization.[24-33] Within the realm of polymer blend research, HTE methodologies have been applied to the synthesis and characterization of gradient thin film libraries, where high-throughput (HT) thin film fabrication techniques enable systematic compositional variation on a single substrate.[29, 34-38] The application of HTE in the realm of PSIBs enables efficient screening of compositions deposited under the same conditions, allowing thorough phase-space exploration and reduced risk of overlooking composition-dependent phenomena.[34, 36-39] Furthermore, the large amount of data generated from HTE can be integrated with data science techniques (e.g. machine learning) to model the relationship between processing conditions and OFET device performance.[40-43]

In this study, we explored the influence of polymer blend composition on the optoelectronic properties of PSIBs employing poly[2,5-(2-octyldodecyl)-3,6-diketopyrrolopyrrole-alt-5,5-(2,5-di(thien-2-yl)thieno [3,2-b]thiophene)] (DPP-DTT) as a model conjugated polymer and polystyrene (PS) as the insulating material to understand how variations in blend composition affect device performance, morphology and phase behavior. To achieve this goal, two complementary approaches, namely high-throughput gradient film (HTGF) and discrete or one-composition-at-a-time (OCAT) methods, were employed. Gradient film libraries covering a wide range of compositions were fabricated to efficiently screen the composition-performance relationship. Characterization of the resultant thin films unveiled unexpected trends and facilitated the observation of onset behaviors and transitions in device performance, morphology and phase behavior as a function of composition. Results obtained using the OCAT method validated the findings and provided a deeper understanding of key composition-performance relationships. Insights revealed through X-ray photoelectron spectroscopy (XPS) depth profiling conducted on OCAT films highlighted the complex interplay between composition and 3D spatial distribution within the film. The generalizability of the gradient approach was confirmed by its application to

poly(3-hexylthiophene) (P3HT) under different solution processing conditions and across a broader composition spectrum.

Results and Discussion

In this study, an HTGF coating apparatus (**Figure 1a**) was used to screen the composition-morphology-performance relationships for the DPP-DTT/PS blends. Operationally, the coating system employs a T-joint mixer design, which is a modification from a previously published apparatus having characteristics of both slot-die and blade coating.[36] To enable gradient film device fabrication, a custom gradient bottom gate bottom contact (BGBC) OFET array was designed, as depicted in **Figure 1b.** Each gradient array contained 60 devices, organized into 4 columns with 15 devices each, whereby each row of 4 devices represents a distinct blend composition and enables quantification of experimental variance. The composition profile was verified for each deposited film coordinate (i.e., each discrete OFET spaced at 4 mm increments) using automated XPS array scans from instrument calibration based on measurements of the S2p signals from DPP-DTT/PS films of known composition (**Figure S1**).

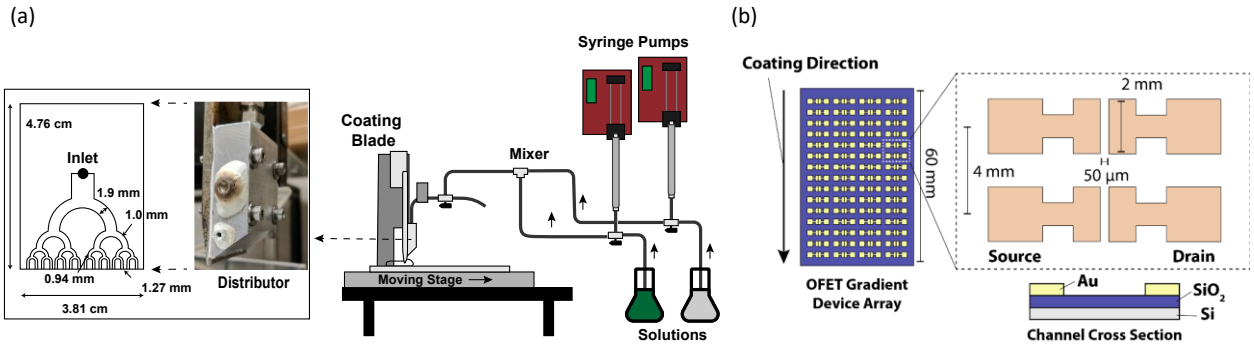

Figure 1. Overview of the HTGF coating system and OFET gradient device array. (a) Schematic flow diagram of the gradient film coating system, including syringe pumps, T-joint mixer, coating blade, distributor and moving stage. The subset shows image and design of microchannel distributor. The apparent mean residence time and mixing volume for this system are 57 s and 0.31 ml respectively. (b) Depiction and schematic of custom-designed transistor array (15 x 4) containing 60 devices per substrate. Reproduced with modifications from Ref. [36]. Copyright 2022 American Chemical Society.

A DPP-DTT/PS gradient film spanning from 0 to 30 wt % DPP-DTT was fabricated by maintaining the temperature of the solution, substrate and HTGF system at 60 °C. Selection of the lower, 0 wt%, bound enabled observation of the onset of charge transport, while the upper bound

was selected based on previous work[8, 11] demonstrating optimal device performance with reduced semiconducting polymer content. The relationship between blend composition and device performance along with corresponding changes in film morphology are presented in **Figure 2**. A total of 83 OFET devices representing distinct blend compositions across one and one-half device arrays was obtained in less than 1 min, with 55 devices exhibiting detectable mobility. The composition and mobility measurements for each coordinate on the DPP-DTT/PS gradient film are presented in **Figure S2.**

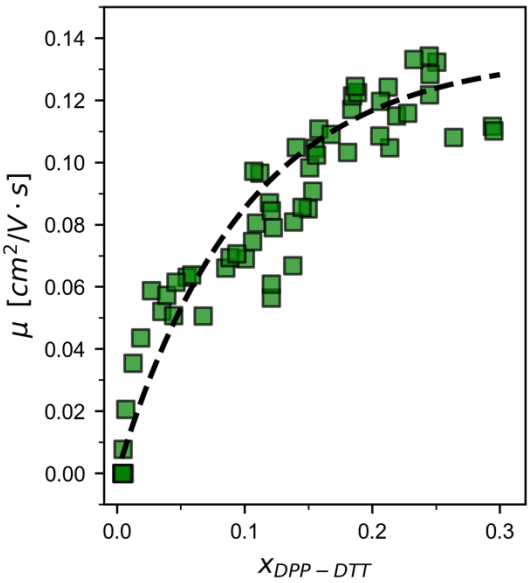

Figure 2. Hole mobility measurements of DPP-DTT/PS devices deposited as gradient thin film libraries. Gradients were prepared using 30/70 DPP-DTT/PS solutions. Dashed trendline represents an exponential fit of y = a[(1-exp(bx)] to facilitate visual comparison, where y is the hole mobility, x is the composition range of DPP-DTT investigated, a = 0.133 and b = -8.98.

Figure 2 illustrates a monotonic increase in hole mobility up to $x_{DPP\text{-}DTT} \sim 0.30$, after which either a plateau or drop in device performance can be expected based on previous findings.[8, 11, 14] Device transfer curves were obtained even at compositions as low as $x_{DPP\text{-}DTT} \sim 0.005$. This observation underscores the advantage of the gradient film methodology to efficiently capture the onset of charge transport in PSIBs. Access to multiple compositions on a single substrate enabled efficient characterization at various points along the gradient film. Furthermore, the gradient approach reduced sample-to-sample variability due to changing environmental conditions, enhancing the reliability and robustness of the acquired data. Atomic force microscopy (AFM) was used to evaluate changes in film surface morphology with increasing composition as presented

in **Figure S3**. A connected network structure around $x_{DPP\text{-}DTT} \sim 0.15$ was observed that may contribute to the observed improved device performance.[8, 11, 14, 44]

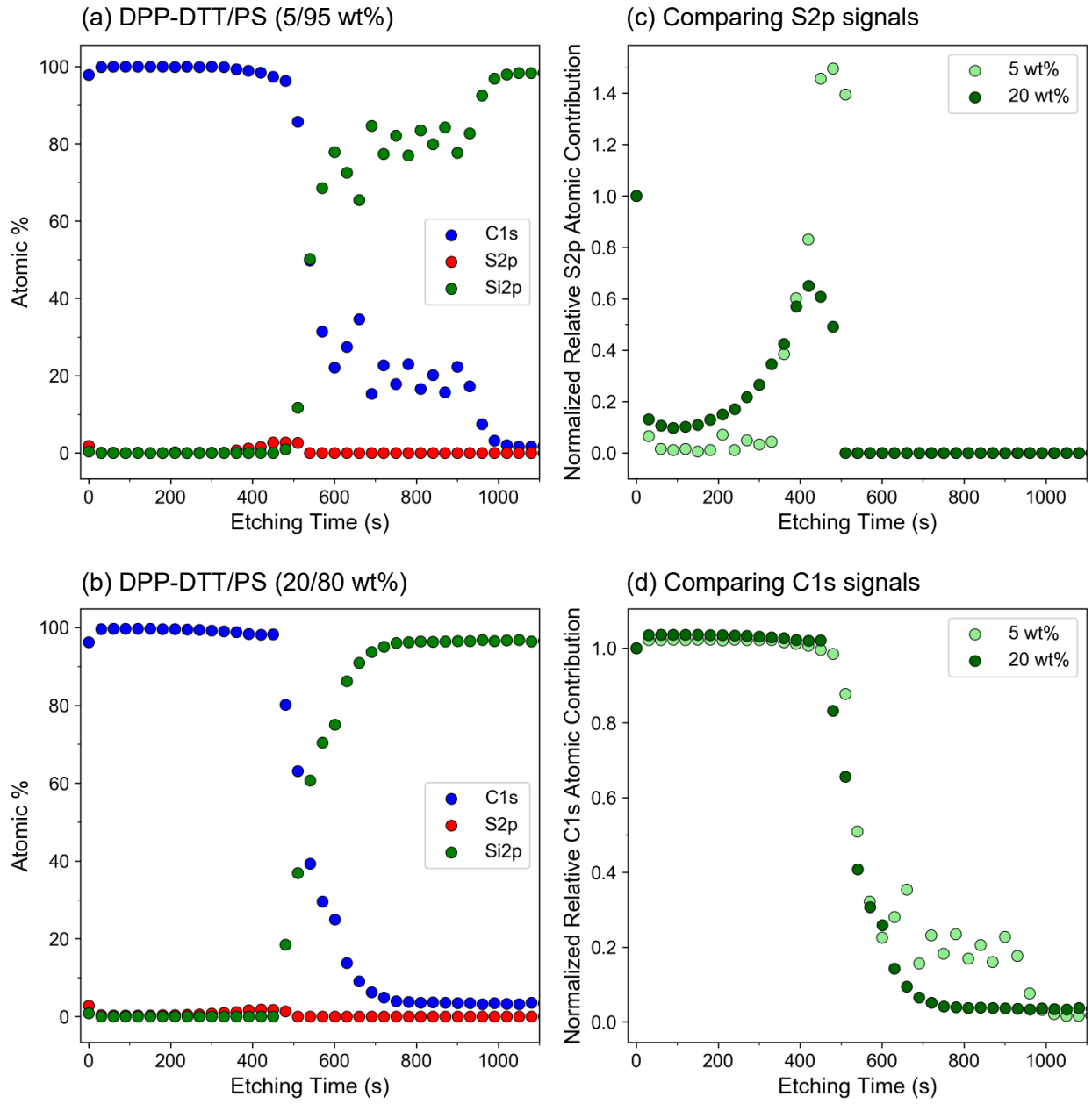

Figure 3. XPS depth profiles of DPP-DTT/PS blends from the gradient film library. (a, b) Atomic percentages of silicon, carbon, and sulfur, determined by the Si2p, C1s, and S2p signals, respectively, plotted against etching time for two different points on the gradient film library with DPP-DTT ratios of 5 wt% (a, top-left) and 20 wt% (b, bottom-left). (c, d) Atomic contributions of sulfur (c, top-right) and carbon (d, bottom-right), determined by the S2p and C1s signals, respectively, plotted against etching time for points on the gradient film library with 5 wt% and 20 wt% DPP-DTT ratios. The S2p/C1s atomic contributions are normalized to the surface level prior to etching (etching time = 0) to compare spectra from different points on the gradient film, accounting for slight differences in film thickness. Etching was

performed at a Ta_2O_5 sputter rate of 0.2 nm/sec. The noise in the carbon and silicon signals in (a) can be attributed to either contamination on the silicon substrate surface or inherent instrumental variations.

The gradient film libraries also provide a convenient platform to investigate changes in polymer distribution through the film thickness as a function of composition. XPS depth profiling provided mechanistic insights in this regard. **Figure 3** presents XPS depth profiles of DPP-DTT/PS blends from the gradient film library, specifically examining points with 5 wt% and 20 wt% DPP-DTT along the gradient. **Figure 3a** and **b** show the atomic contributions of carbon (representative of both DPP-DTT and PS) from the C1s signal, sulfur (representative of DPP-DTT) from the S2p signal, and silicon (representative of the silicon substrate) from the Si2p signal at different etching times for two points on the gradient film library with DPP-DTT ratios of 5 wt% and 20 wt% respectively. Given that sulfur is present only in DPP-DTT (**Figure S4**), it serves as a qualitative indicator of the proportion of DPP-DTT at different depths within the blend film. Note that although nitrogen and oxygen are exclusive to DPP-DTT, they were not used as unique identifier elements in this study, considering their potential for physisorption at the surface.[45, 46] Additionally, based upon the molecular structure of DPP-DTT, the atomic contribution of nitrogen and oxygen is considerably lower compared to sulfur. **Figure 3c** and **d** compare the normalized relative atomic contributions of sulfur and carbon, respectively, for the two points of interest at different depths within the blend films. In both blends, the sulfur signal (**Figure 3c**) appeared to decrease precipitously during the initial stages of etching, followed by a sustained low level within the bulk, subsequently increasing in the range of 250 – 300 s to peak around 450 s as etching progressed towards the film-substrate interface. To delve deeper into the rapid initial decrease in sulfur, additional etching was conducted at a slower rate on another 20 wt% DPP-DTT sample point from the same gradient, focusing specifically on etching only the initial few layers (~10 nm) of the film, with the results depicted in **Figure S5**. The slower etching rate revealed a more gradual decrease in the sulfur signal, providing confirmation of diminishing DPP-DTT content as the film's bulk was approached. In both instances, carbon (**Figure 3d**) was detected throughout the film thickness, diminishing towards the film-substrate interface, suggesting the presence of mainly polystyrene throughout the bulk. These results unveil the presence of a PSIB layer comprising DPP-DTT and PS at the air-film interface, the presence of mainly polystyrene in the bulk, while the film-substrate interface again presents with DPP-DTT and some proportion of PS, suggesting a pattern of vertical tri-layer phase separation (semiconductor/insulator/semiconductor), a

phenomenon previously observed in other blended conjugated polymer systems.[3, 15, 47-53] Additionally, it is noteworthy that as the composition increases from 5 wt% to 20 wt% DPP-DTT, there is a slight increase in the proportion of DPP-DTT within the bulk film, with virtually no DPP-DTT detected in the bulk at 5 wt%.

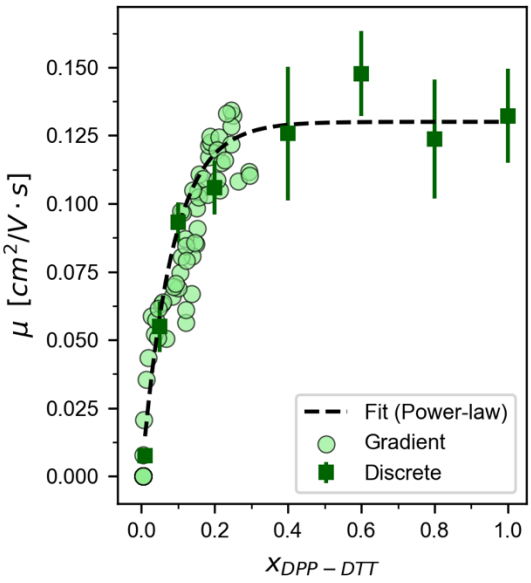

Figure 4. Comparison plot of OFET hole mobilities for gradient films (circles) and OCAT blade-coated films (squares) of DPP-DTT/PS blends at varying wt% of DPP-DTT. Dashed trendline represents an exponential fit of y = a[(1-exp(bx)] to facilitate visual comparison, where y is the hole mobility, x is the composition range of DPP-DTT investigated, a = 0.132 and b = -10.45.

The insights obtained from the gradient film results were validated by OCAT experiments. Blend solutions of DPP-DTT/PS at various compositions, both within and outside the gradient range, were prepared and blade-coated onto glass and silicon BGBC OFET substrates for relevant characterization. **Figure 4** provides a comparison plot of the average OFET hole mobilities obtained from blade-coated OCAT films and gradient films prepared using the HTGF coater (*vide supra*). Notably, within the composition range selected for the preliminary gradient experiments, the mobilities from the OCAT films are consistent with those fabricated using the gradient method. These results underscore the efficacy of the gradient film in accurately capturing the composition-device performance trends. Moreover, following the anticipated monotonic increase, the mobility of the OCAT devices gradually reached a plateau at compositions exceeding 40 wt% DPP-DTT.

The onset of the plateau can be identified as the optimal composition for improved device performance while minimizing the more expensive semiconducting component. The mobilities presented in **Figure 4** for the OCAT films were extracted from the forward transfer curve, with similar results observed for mobilities extracted from the backward transfer curve (**Figure S6**). The OFET device transfer and output curves for the OCAT experiments are provided in **Figures S7** and **S8**, respectively. Additionally, **Table S1** tabulates extracted average threshold voltage (V_{th}) and I_{on}/I_{off} ratios for the OCAT films as a function of blend composition. Devices fabricated from low wt% DPP-DTT exhibited higher I_{on}/I_{off} ratios, while the threshold voltage showed no obvious trend, remaining within the desired range between -20 and 20V.

The consistent OFET mobility of the PSIB films at low compositions of DPP-DTT (~20-40 wt%) and its similarity to the mobility observed at 100 wt% DPP-DTT has been observed previously.[8, 11, 14] The phenomenon has been attributed to the formation of a connected, semiconducting polymer network structure within the PS matrix, [8, 11, 14, 44] as evidenced here by AFM (**Figure S9**). Similar to the gradient results, OCAT films exhibited gradual formation of a networked structure that increased in density as the DPP-DTT content increased to 80 wt%, eventually forming an apparently amorphous and featureless film at 100 wt% DPP-DTT. The connected network morphology observed in DPP-DTT/PS blend films could provide percolation pathways for charge carriers, improving charge transport within the film.[8, 9, 15] Furthermore, organic/polymer transistors are interface-driven devices, wherein charge transport predominantly occurs within a thin semiconductor layer at the semiconductor/dielectric interface connecting the source and drain electrodes.[3, 54, 55] As observed by XPS depth profiling (**Figure 3**)**,** the formation of a more contiguous DPP-DTT enriched layer at the substrate interface may be the key factor that enables blend films with low weight fractions of DPP-DTT to exhibit charge carrier mobilities that approach those of the 100 wt% semiconductor films.[3] The influence of blend composition on the solid-state polymer chain excitonic interactions for the OCAT DPP-DTT/PS films was also investigated using UV-Vis absorption spectroscopy. **Figure S10** presents the spectra of DPP-DTT/PS blend films at discrete compositions ranging from 20 to 100 wt% DPP-DTT and reveals a spectral red shift associated with decreasing DPP-DTT content, which is attributed to intermolecular π-π stacking and points to a more planarized conjugated backbone in films

comprising lower wt% DPP-DTT.[56, 57] The slight increase in intensity of the shoulder at 830 nm suggests that PS facilitates DPP-DTT aggregation during film formation.[8]

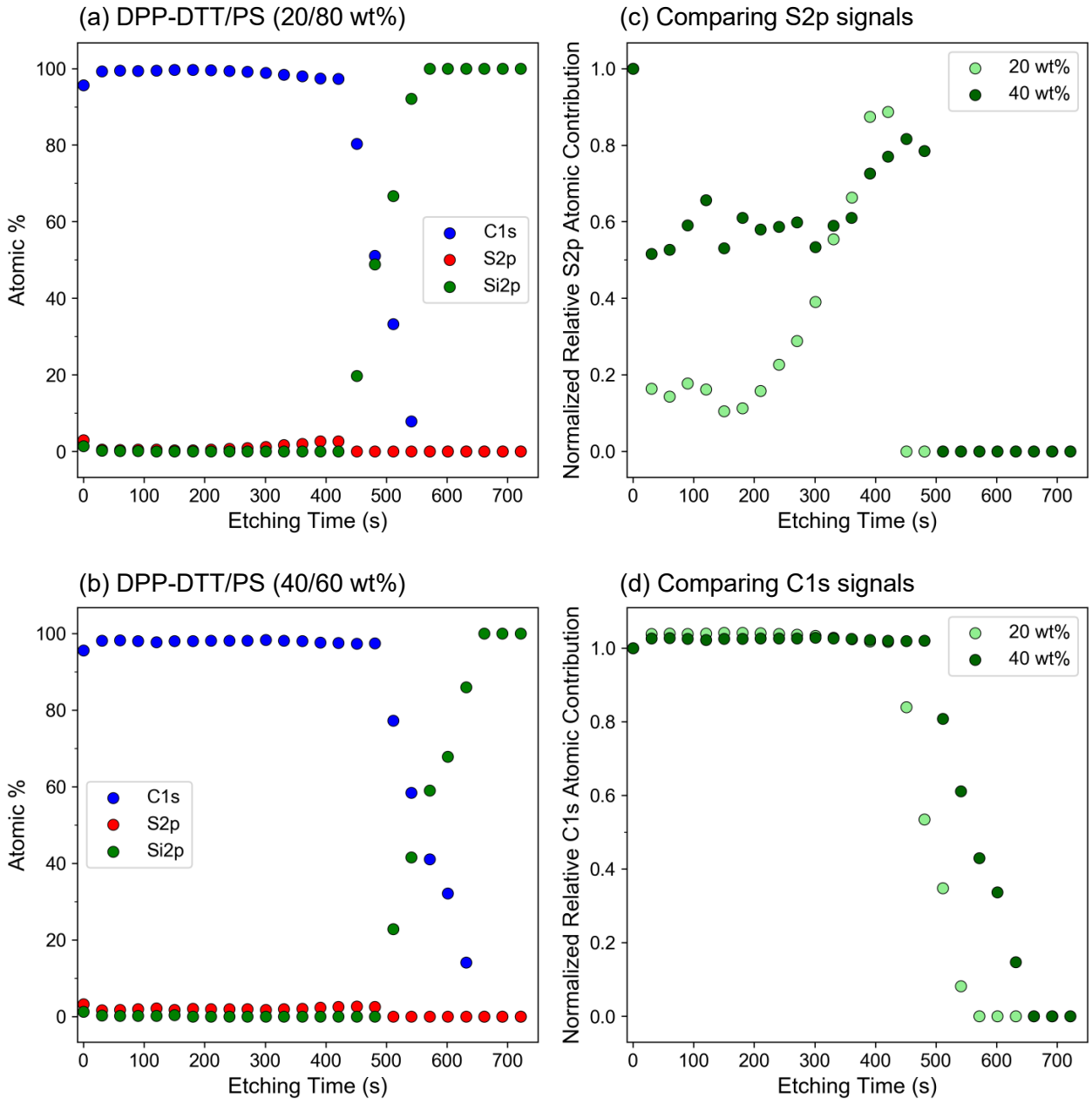

Figure 5. XPS depth profiles of DPP-DTT/PS blends from the OCAT blend films. (a, b) Atomic percentages of silicon, carbon, and sulfur, determined by the Si2p, C1s, and S2p signals, respectively, plotted against etching time for OCAT blend films with DPP-DTT ratios of 20 wt% (a, top-left) and 40 wt% (b, bottom-left). (c, d) Atomic contributions of sulfur (c, top-right) and carbon (d, bottom-right), determined by the S2p and C1s signals, respectively, plotted against etching time for OCAT blend films with DPP-DTT ratios of 20 wt% and 40 wt%. The S2p/C1s atomic contributions are normalized to the surface level prior to

etching (etching time = 0) to compare spectra from different OCAT films, accounting for differences in film thickness. Etching was performed at a Ta2O5 sputter rate of 0.2 nm/sec.

XPS depth profiling was also conducted on the OCAT films (**Figure 5**) to validate and explore insights gained from the gradient experiments, specifically focusing on the observed vertical phase separation phenomenon (**Figure 3**). **Figure 5a** and **b** show the atomic contributions of carbon, sulfur, and silicon at different etching times for the 20 and 40 wt% DPP-DTT/PS OCAT films respectively. Results from depth profiling a 100 wt% DPP-DTT film are also presented in **Figure S11**. It can be observed from **Figure 5** that for the 20 wt% and 40 wt% blend films, the silicon substrate was reached after etching for approximately 450 and 500 s, respectively. The slight differences in the required etching time may be attributed to variations in film thickness (**Figure S12**). **Figure 5c** reveals that in the 20 wt% DPP-DTT case, the etching profile appears similar to that of the gradient film (**Figure S13**), again suggesting that at 20 wt% DPP-DTT, the blend undergoes vertical, tri-layer phase separation. The slight differences in signal intensity may be due to variations in film thickness resulting from the different coating techniques used. The gradient film approach utilizes a combination of slot die and blade coating techniques, whereas the OCAT approach relies solely on blade coating. The 40 wt% DPP-DTT film also displayed the presence of the semiconducting component at the air and substrate interfaces. In behavior that is consistent with reported findings,[8, 11] the sulfur signal in the bulk of the film (**Figure 5c**) appeared higher than that observed for the film prepared with only 20 wt% DPP-DTT, suggesting a more uniform distribution of the semiconducting component throughout the film. A similar observation was made by Xu et al.[52] for blends of poly[3,6-di-2-thienyl-pyrrolo[3,4-c]pyrrole-1,4-dione-alt-thieno[3,2-b]thiophene] (DPPT-TT) and polystyrene-block-poly(ethylene-co-butylene)-block-polystyrene (SEBS). At low DPPT-TT compositions, vertical tri-layer phase separation was observed, where the semiconducting component appeared to segregate at the air and substrate interfaces with SEBS primarily occupying the bulk of the film; and as the proportion of DPPT-TT increased, a more uniform distribution was observed throughout.

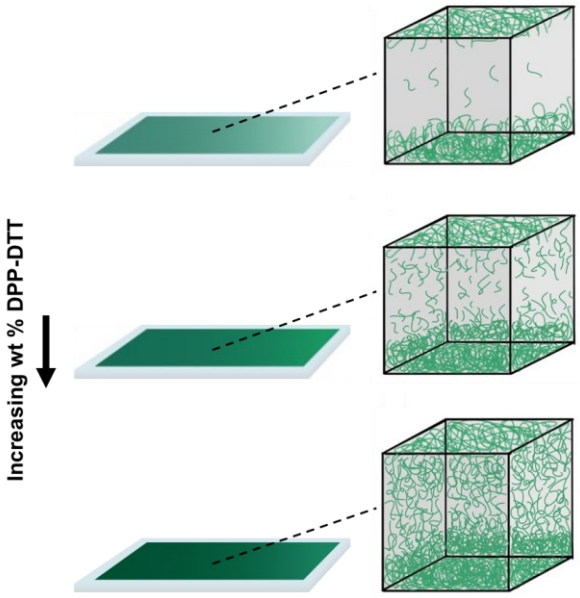

Figure 6. Illustration of the potential phase separation mechanism occurring during film formation. The green chains represent domains of DPP-DTT, while the grey space represents PS. At lower compositions there is an enrichment of DPP-DTT at the air/film and film/substrate interface, with majority of the film bulk containing PS. As the ratio of DPP-DTT within the film increases, a more uniform distribution of the two polymers within the film is observed.

From a mechanistic perspective and as illustrated in **Figure 6**, the observed accumulation of DPP-DTT at the air and substrate interfaces is most likely driven by energy minimization,[3, 15, 58, 59] in addition to factors such as polymer intrinsic characteristics[51, 60] and deposition conditions.[8, 11, 44] Given that reported solubility parameters for DPP-DTT, PS, and chlorobenzene are similar,[8, 11] the apparent vertical phase separation observed here may also be due to the substantial differences in DPP-DTT (~200 kDa) *vs.* PS (~37 kDa) molecular weight,[51, 61] high polydispersity (~3) of DPP-DTT,[60] polymer solution characteristics,[12, 62-64] parameters associated with blend film fabrication,[8, 11, 44, 65, 66] and other factors.[3, 15, 22] An increase in wt% of DPP-DTT within the film leads to a more substantial proportion of DPP-DTT in the bulk, suggesting a more uniformly distributed blend;[8, 11, 52] however, DPP-DTT continues to be enriched at both the substrate and air interfaces. Most likely, the observed DPP-DTT increase in the bulk of the film is linked to the length scale of phase separation, whereby the XPS sampling spot size (400 μm) is sufficiently large to encompass both polymer domains. At higher wt% DPP-DTT, the phase separated polymer blend may comprise a more dense, DPP-DTT networked structure within the bulk parallel to the substrate.[8, 11] Clearly, phase separation in PSIBs is a complex phenomenon that depends on a multitude of parameters. As a consequence, optimization of the blend systems requires careful

selection of materials and processing conditions to match desired performance targets.[67] Further, additional studies to elucidate conjugated polymer blend phase behavior will be invaluable.

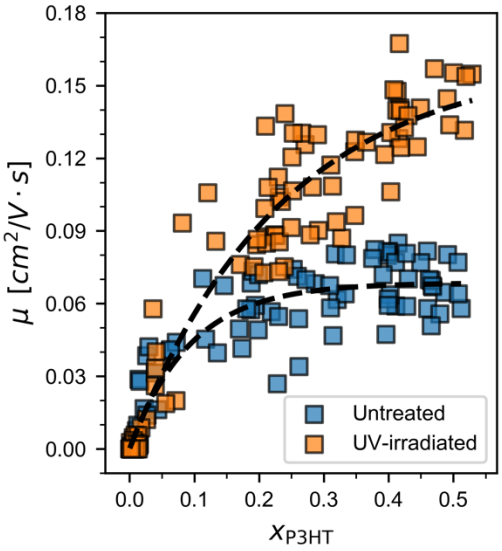

Figure 7. Hole mobility measurements of P3HT/PS devices deposited as thin film libraries. Final solutions were either derived from 50/50 P3HT/PS solutions that were either used as dissolved without treatment (untreated) or UV-irradiated for 8 minutes prior to loading. Dashed trendline represents an exponential fit of y = a[(1-exp(bx)] to each dataset to facilitate visual comparison, where y denotes the hole mobility, x signifies the P3HT wt% investigated, and a and b are constants derived from the fit. In the case of the untreated system, a = 0.068 and b = -10.65, while for the UV-irradiated system, a = 0.16 and b = -4.24.

Expanding beyond DPP-DTT/PS, the HTGF coater was also used to investigate blends of untreated and UV-irradiated chloroform solutions of P3HT/PS at room temperature, showcasing the generalizability of the approach. UV-irradiated P3HT/PS blend solutions were prepared alongside untreated alternatives to assess the ability of the HTGF approach to capture the effects on performance of pre-processing the blend solution prior to film deposition.[1, 68, 69] The resulting composition-device performance relationships and changes in film morphology are illustrated in **Figure 7**. Screening of untreated and UV-irradiated P3HT/PS was conducted at room temperature by generating composition libraries spanning 0–50 wt% P3HT, where composition boundaries were chosen based on previous work.[1] Composition calibration curves are provided in **Figure S14**, while composition and mobility measurements for each coordinate on both gradient films are presented in **Figure S15** and **S16.** Over 100 OFET devices, encompassing distinct blend compositions distributed across two arrays, were fabricated. The composition-mobility profiles derived from the gradient device screening (**Figure 7**) highlights a distinct enhancement in FET

hole mobility when devices are fabricated from UV-irradiated solutions. This differentiation becomes particularly pronounced as the two exponential trendlines begin to diverge at compositions exceeding 10-15 wt% P3HT. Both sets of devices initially exhibit a positive and incremental trend in mobility. **Figure S17** provides a closer look at the behavior when the proportion of P3HT is below 10 wt%, where both pristine and UV-irradiated gradient libraries display similar behavior. For both sets of P3HT films, device transfer curves were measurable at compositions even below 1 wt% P3HT, with those from the UV-irradiated solutions showing a greater frequency of measurable devices (non-zero mobility). As the composition exceeds past 10 wt% P3HT, the mobility of the untreated devices gradually reaches a plateau at compositions above 40 wt% P3HT (**Figure 7**). Conversely, devices produced from UV-irradiated solutions displayed continuous mobility improvement with increasing wt% P3HT. These findings align well with the trends observed in previous studies.[1] The enhanced performance of the devices fabricated from the UV-irradiated blend solutions in this study can be attributed to the formation of ordered P3HT nanofibrillar structures that create pathways between P3HT regions within the film, thereby facilitating charge transport across the channel.[1] As reported by Chang, *et al*.,[1, 68] UV irradiation of P3HT in chloroform solution may induce a conformational change of the polymer main chain from an aromatic to a quinoidal-like structure, promoting favorable π–π interchain interactions leading to self-assembled fibrillar aggregates. These aggregates persist through the coating process, appearing as ordered nanofibrillar structures in the resultant P3HT/PS blend thin films, thereby improving charge transport and device performance.[1, 68, 69]

The compositional library was also interrogated at selected coordinates using AFM to connect the evolution in thin film morphology to corresponding improvements in device performance as shown in **Figure S18**. The lowest wt% P3HT films ($0 < x_{P3HT} < 0.1$) are associated with an initial appearance of P3HT droplet-like features approximately 100 nm in size **(Figure S19)**. Eventually, as the proportion of P3HT increases, these droplets grow in size and overlap, developing into island-like morphologies that evolve into a more bi-continuous network. The untreated films display smoother, more globular P3HT phase boundaries, while UV-irradiated films show jagged P3HT structures that appear to provide more interconnectivity between domains (**Figure S18**). This increased interconnectivity in the UV-irradiated films supports the observed enhancement in charge transport.[1] Additionally, depth profiling conducted

on the untreated P3HT/PS film at two distinct composition points unveiled a trend similar to that observed for DPP-DTT/PS gradients. **Figure S20** validates the existence of apparent vertical phase separation, demonstrating a noticeable increase in the proportion of P3HT within the bulk of the film as the proportion of P3HT increases from 5 to 50 wt%.

Similar to the DPP-DTT/PS system, OCAT experiments were performed for P3HT/PS, encompassing blend compositions within and outside of the original range of the library. The OCAT films were analyzed for device performance (**Figure S21 – S25**, **Table S2**, and **Table S3**), morphology (**Figure S26**), spectroscopic behavior (**Figure S27**), and composition profile through the thickness of the films (**Figure S28** and **Figure S29**). The observed trends closely align with the gradient results. When comparing the gradient film and OCAT OFET mobility results (**Figure S28**), it becomes evident that the mobilities derived from the gradient film approach consistently outperform the OCAT results by a factor of 2 to 3 across the investigated composition range. These differences are attributed to inherent mechanistic distinctions linked to the two coating methods: the gradient film approach utilizes a slot die + blade coating technique, whereas the OCAT approach relies strictly on blade coating. It is hypothesized that flow-induced nucleation of fibril-like aggregates might occur during the mixing stage or while passing through the distributor in the gradient film system, potentially leading to the self-assembly of P3HT morphological motifs conducive to higher mobilities.[70] In addition to composition and coating methodology, the impact of, and possible synergies between, other processing parameters such as aging time,[71, 72] coating speed,[44, 73] channel orientation,[74] and deposition temperature,[75-77] etc., remain to be investigated. This underscores the importance of incorporating high-throughput experiments into the existing paradigm to systematically explore and optimize each variable in the OFET processing space.

Conclusion

In this work, an exploration of PSIBs achieved through a HTGF library approach, coupled with traditional discrete experiments, revealed key insights into the relationships between blend composition, thin-film morphology, phase-separation and device performance. The HTGF approach allowed for efficient screening of a broad composition range of DPP-DTT blends with PS as the insulating material. Clear advantages in capturing the nuances of onset behaviors and

transitions in device performance, phase separation and morphology based on composition were demonstrated. Such aspects can often be elusive, making the HTGF approach valuable for gaining a comprehensive understanding of PSPRs in PSIBs. The insights from the gradient approach were also investigated and validated through OCAT experiments, which provided a targeted approach to investigate specific blend compositions within and beyond the gradient range. The OCAT trends observed for DPP-DTT agreed with those from the gradient films, highlighting the effectiveness of the gradient approach in capturing key PSPRs in PSIBs. XPS depth profiling unveiled findings such as the presence of DPP-DTT at air interface, with enrichment of DPP-DTT at the substrate interface at lower blend ratios of the semiconducting component, transitioning to a more even distribution within the bulk at higher blend ratios. The gradient approach was also employed with P3HT/PS blends under different solution processing conditions and spanning a wider composition range. The outcomes validated the versatility of the HTGF approach, demonstrating its applicability to diverse conjugated polymer blend systems. The observed device performance differences between HTGF and OCAT coated films for DPP-DTT vs. P3HT point to the impact of polymer molecular structure on the solution behavior of semiconducting polymers during the thin film deposition process, particularly under dynamic flow conditions. The results emphasize the complexity PSIBs and support the critical need to develop effective high-throughput characterization techniques such as automated microscopy, spectroscopy, and device testing. Access to such methods to efficiently unravel the behavior of these complex systems will expedite their scalability and deployment for practical applications.

Materials and Methods

Materials

Poly[2,5-(2-octyldodecyl)-3,6-diketopyrrolopyrrole-alt-5,5-(2,5-di(thien-2-yl)thieno [3,2-b]thiophene)] (DPP-DTT) (Mw = 204 kDa, PDI = 3.09, Ossila Ltd) kDa, Poly(3-hexylthiophene) (P3HT) (Mw = 74 kDa, RR = 95%, Rieke Metals, Inc.), polystyrene (PS) (Mw = 37 kDa, MilliporeSigma), chloroform (MilliporeSigma, anhydrous, amylenes as stabilizer) and chlorobenzene (anhydrous, Sigma-Aldrich) were used as obtained.

High-throughput gradient coater design

The coating system employed in this study represents a minor modification of a previously described gradient pumping system design,[36] with the only difference being the replacement of the

herringbone mixer with a 1/8-inch, T-joint union (Swagelok, SS-41GXS2). The polymer solutions are introduced into the T mixer positioned at the convergence of the two inlet streams. At this point, mixing is facilitated by the fitting and the collision of the two feeds. The remaining components of the coating system remained unchanged.

Organic field-effect transistor substrate fabrication

Heavily n-doped silicon wafers, with a 300 nm layer of thermally grown SiO_2, were purchased from Rogue Valley Microdevices. Source and drain electrodes were deposited on the SiO_2 dielectric layer via standard photolithography lift-off techniques followed by E-beam evaporation of a 3 nm Cr adhesion layer and 50 nm Au for the contacts, in a bottom-gate bottom-contact device configuration. This approach was used with different photomask designs to fabricate the standard OFET devices for one-at-time experimentation as well as the OFET gradient device array (**Figure 2b**).

Constant composition film sample preparation for one-at-a-time experiments

Prior to film deposition, substrates were cleaned by sequential sonication in acetone, methanol, and isopropanol (10 min each), followed by cleaning in UV–ozone for 30 min (Novascan PSD-UV).

The preparation of DPP-DTT/PS samples at different blend ratios involved the initial preparation of a stock solution of 7 g/L by dissolving DPP-DTT in chlorobenzene at 100 °C for 4 hours, followed by continued heating at 56 °C overnight. Similarly, a polystyrene (PS) solution at 7 g/L was prepared by dissolving polystyrene pellets in chlorobenzene at 60 °C for 30 minutes. Blend solutions at varying compositions were then obtained by mixing the DPP-DTT and PS stock solutions at desired ratios. To prepare DPP-DTT/PS thin films for the OCAT experiments, the blend solutions were blade-coated onto glass and OFET substrates at a temperature of 56 °C, with a shearing speed of 2 mm/s, followed by annealing at the same temperature for 10 minutes.

The preparation of P3HT/PS samples at different blend ratios involved the initial preparation of separate stock solutions (10 g/L) of P3HT and PS dissolved in chloroform at 55°C for 30 minutes. Blend solutions at varying compositions were then obtained by mixing the P3HT and PS stock solutions at desired ratios. The blend solutions were further pre-processed by UV-irradiation using a handheld lamp (Entela, Model UVGL-15, 5 mW cm^{-2} , 254 nm) for 8 minutes according to the procedure in Chang et al.[1] To create P3HT/PS thin films for the one-composition-at-a-time experiments, the blend solutions were blade-coated onto glass (Electron Microscopy Sciences) and OFET substrates at a temperature of 25 °C, with a shearing speed of 2 mm/s, followed by annealing at the same temperature for 10 minutes.

Gradient film sample preparation

DPP-DTT/PS blend solutions were first prepared and dissolved in chlorobenzene at the desired blend ratio (30 wt% DPP-DTT). Films were coated onto OFET gradient arrays using the HTGF coater. First, a cleaning procedure was followed in which the system at 60 °C was flushed with chlorobenzene (2-3 runs) and air (2 runs) to remove any residual material. The syringes feeding

the flow system were then filled with DPP-DTT/PS (blend ratio of 30 wt% DPP-DTT) and PS solutions. Prior to coating, the system was initially infused with PS solution until droplets at a consistent drip rate were visible at the outlet purge. Next, approximately 0.3 ml of the DPP-DTT/PS solution was pumped into the system so that the blend solution reached the mixer. The PS was then pumped at the maximum flow rate to remove excess blend solution until colored droplets of blend solution appeared at the outlet purge followed by clear PS solution. Once the substrates had been cleaned and positioned under the distributor outlet, the pump containing the DPP-DTT/PS blend solution was set to a constant flow rate of 20 mL/h and the blend solution was continuously infused into the system. Prior to diverting flow to the distributor for film coating, flow was directed to the purge stream for a prescribed initial delay period of 10 s. Once the desired length of the substrate was coated, pump flow was paused, stage position reset, and a the substrate was replaced before flow was resumed.

The constant composition flow coated samples that were prepared for the composition calibration curves where coated in the same manner, without flowing any PS solution. P3HT/PS pristine and UV-irradiated gradient films were prepared in the same manner, with the only difference being the use of chloroform as the solvent instead of chlorobenzene and the system was maintained at room temperature.

OFET Characterization

Field-effect transistor properties were measured in a nitrogen glovebox by use of an Agilent 4155c semiconductor parameter analyzer. The charge carrier mobilities and threshold voltages were calculated in the saturation regime (V_{GS} = -80 V with V_{DS} swept from 80 to -80 V) by fitting the following equation to the transfer curves of drain current (I_{DS}) versus gate voltage (V_{GS}):

$$I_{DS} = \frac{WC_{OX}}{2L}\mu(V_{GS} - V_T)^2$$

where W is channel width (50 μm), L is channel length (2000 μm), C_{OX} is capacitance per unit area of the SiO_2 dielectric layer (1.15×10^{-18} F·cm^{-2}), μ is the hole mobility, and V_T is threshold voltage. The on/off ratio was calculated as the maximum drain current measured when a negative bias is applied, divided by the minimum drain current measured when a positive bias is applied.

UV-visible spectroscopy (UV-vis)

Steady-state linear absorption measurements were performed using a Cary 5000 UV−Vis−NIR spectrometer in transmission mode for the solid thin-films deposited on glass substrates.

X-ray photoelectron spectroscopy (XPS)

The composition across different points of the gradient thin film samples were obtained using X-ray photoelectron spectroscopy (XPS) using a Thermo K-Alpha XPS system equipped with a monochromatic Al-K X-ray source (1468 eV). Spectra were collected using a flood gun with high purity Argon gas and an X- ray spot size of 400 μm. Survey scans were collected with pass energy of 200 eV with 1 eV increments. High resolution point and line scans for C1s, Si2p and S2p were

collected with pass energy of 50 eV with 0.1 eV increments. The element distributions in the blend films were analyzed using the depth profiling feature (40-50 etches, 30 seconds per etch, Sputter Rate Estimate : Ta_2O_5 = 0.20 nm/sec).

Atomic force microscopy (AFM)

Atomic force microscopy (AFM) images were obtained on thin film samples using a Bruker Dimension Icon AFM in tapping mode with n-type silicon tips (HQ:NSC14/NoAl, 160 kHz, 5 N/m, MikroMasch).

Profilometry

Thickness of the PSIB thin films on glass substrates was obtained using a Bruker DekakXT profilometer.

ASSOCIATED CONTENT

Supporting Information

The supporting information is available free of charge at:

Calibration curves for blend composition determination; Polymer chemical structures; XPS depth profiling schematic; OFET transfer and output characteristics; AFM images for Gradient and OCAT films, UV-Vis spectroscopy results for OCAT films, Profilometry results.

AUTHOR INFORMATION

Corresponding Authors

Carson Meredith – School of Chemical & Biomolecular Engineering, Georgia Institute of Technology, 311 Ferst Drive, Atlanta, GA, 30332. Email: carson.meredith@chbe.gatech.edu

Martha A. Grover – School of Chemical & Biomolecular Engineering, Georgia Institute of Technology, 311 Ferst Drive, Atlanta, GA, 30332. Email: martha.grover@chbe.gatech.edu

Elsa Reichmanis – Department of Chemical & Biomolecular Engineering, Lehigh University, 124 E. Morton Street, Bethlehem, PA 18015. Email: elr420@lehigh.edu

Other Authors

Aaron L. Liu - School of Chemical & Biomolecular Engineering, Georgia Institute of Technology, 311 Ferst Drive, Atlanta, GA, 30332;

Haoqun Zhao – School of Chemical & Biomolecular Engineering, Georgia Institute of Technology, 311 Ferst Drive, Atlanta, GA, 30332; School of Chemical Engineering, University of Minnesota, Amundson Hall, 421, Washington Ave SE, Minneapolis, MN, 55455

Rahul Venkatesh – School of Chemical & Biomolecular Engineering, Georgia Institute of Technology, 311 Ferst Drive, Atlanta, GA, 30332

Yulong Zheng – School of Chemistry and Biochemistry, Georgia Institute of Technology, 801 Atlantic Drive, Atlanta, GA, 30332

ORCID:
Elsa Reichmanis: 0000-0002-8205-8016
Martha Grover: 0000-0002-7036-776X
Carson Meredith: 0000-0003-2519-5003

Rahul Venkatesh: 0000-0003-1008-6568
Yulong Zheng: 0000-0001-5136-1971
Aaron L. Liu: 0000-0001-7347-5347
Haoqun Zhao: 0000-0002-3871-0302

Notes
The authors declare no conflict of interest.

Acknowledgments

The authors would like to acknowledge the National Science Foundation Grant No. 1922111, DMREF: Collaborative Research: Achieving Multicomponent Active Materials through Synergistic Combinatorial, Informatics-enabled Materials Discovery for support. This work was performed in part at the Georgia Tech Institute for Electronics and Nanotechnology, a member of the National Nanotechnology Coordinated Infrastructure (NNCI), which is supported by the National Science Foundation (ECCS-2025462); E.R. appreciates support associated with Carl Robert Anderson Chair funds at Lehigh University. The authors appreciate Priyal Shah for designing the illustration of the phase separation mechanism observed in Figure 6 and the Table of Contents graphic. The authors would also like to extend their gratitude to Dr. Miguel Gonzalez for his invaluable expertise and guidance in analyzing XPS depth profiling results.

Table of Contents (TOC) Graphic

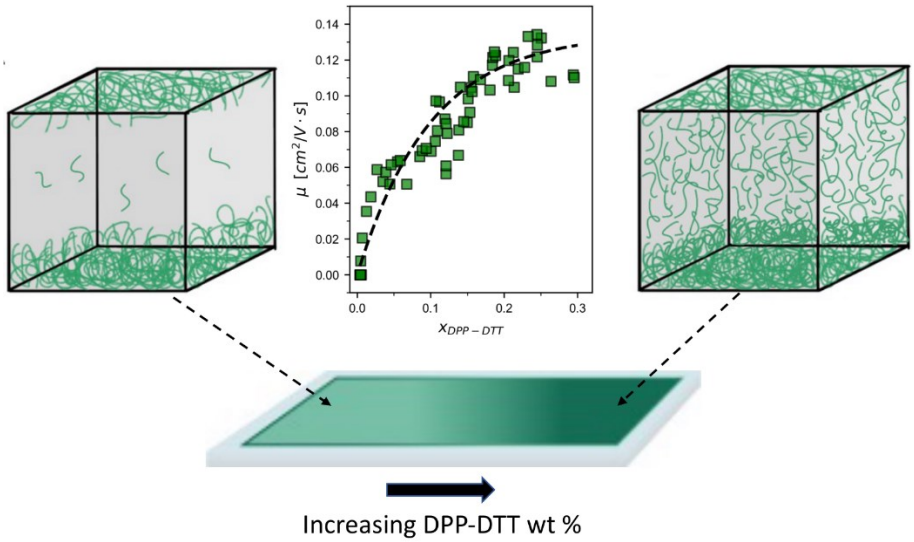

REFERENCES

1. Chang, M.; Choi, D.; Wang, G.; Kleinhenz, N.; Persson, N.; Park, B.; Reichmanis, E., Photoinduced Anisotropic Assembly of Conjugated Polymers in Insulating Polymer Blends. *ACS Applied Materials & Interfaces* **2015,** *7* (25), 14095-14103.
2. Choi, D.; Kim, H.; Persson, N.; Chu, P.-H.; Chang, M.; Kang, J.-H.; Graham, S.; Reichmanis, E., Elastomer–Polymer Semiconductor Blends for High-Performance Stretchable Charge Transport Networks. *Chemistry of Materials* **2016,** *28* (4), 1196-1204.
3. Kang, B.; Ge, F.; Qiu, L.; Cho, K., Effective Use of Electrically Insulating Units in Organic Semiconductor Thin Films for High-Performance Organic Transistors. *Advanced Electronic Materials* **2017,** *3* (2), 1600240.
4. McBride, M.; Persson, N.; Keane, D.; Bacardi, G.; Reichmanis, E.; Grover, M. A., A Polymer Blend Approach for Creation of Effective Conjugated Polymer Charge Transport Pathways. *ACS Appl Mater Interfaces* **2018,** *10* (42), 36464-36474.
5. Nam, M.; Lee, C.; Ko, D.-H., Sequentially processed quaternary blends for high-performance indoor organic photovoltaic applications. *Chemical Engineering Journal* **2022,** *438*, 135576.
6. Pan, Y.; Yu, G., Multicomponent Blend Systems Used in Organic Field-Effect Transistors: Charge Transport Properties, Large-Area Preparation, and Functional Devices. *Chemistry of Materials* **2021,** *33* (7), 2229-2257.
7. Root, S. E.; Savagatrup, S.; Printz, A. D.; Rodriquez, D.; Lipomi, D. J., Mechanical Properties of Organic Semiconductors for Stretchable, Highly Flexible, and Mechanically Robust Electronics. *Chemical Reviews* **2017,** *117* (9), 6467-6499.
8. Lei, Y.; Deng, P.; Li, J.; Lin, M.; Zhu, F.; Ng, T.-W.; Lee, C.-S.; Ong, B. S., Solution-Processed Donor-Acceptor Polymer Nanowire Network Semiconductors For High-Performance Field-Effect Transistors. *Scientific Reports* **2016,** *6* (1), 24476.

9. Nikzad, S.; Wu, H.-C.; Kim, J.; Mahoney, C. M.; Matthews, J. R.; Niu, W.; Li, Y.; Wang, H.; Chen, W.-C.; Toney, M. F.; He, M.; Bao, Z., Inducing Molecular Aggregation of Polymer Semiconductors in a Secondary Insulating Polymer Matrix to Enhance Charge Transport. *Chemistry of Materials* **2020,** *32* (2), 897-905.
10. Qiu, L.; Lee, W. H.; Wang, X.; Kim, J. S.; Lim, J. A.; Kwak, D.; Lee, S.; Cho, K., Organic Thin-film Transistors Based on Polythiophene Nanowires Embedded in Insulating Polymer. *Advanced Materials* **2009,** *21* (13), 1349-1353.
11. Wei, P.; Shen, Z.; Qin, X.; Zhang, P.; Bu, L.; Chen, Q.; Roth, S. V.; Lu, G., Improving Charge Injection at Gold/Conjugated Polymer Contacts by Polymer Insulator-Assisted Annealing for Transistors. *Small* **2022,** *18* (9), 2105896.
12. Zhang, G.; Lee, S.; Gutiérrez-Meza, E.; Buckley, C.; McBride, M.; Valverde-Chávez, D. A.; Kwon, Y. H.; Savikhin, V.; Xiong, H.; Dunn, T. J.; Toney, M. F.; Yuan, Z.; Silva, C.; Reichmanis, E., Robust and Stretchable Polymer Semiconducting Networks: From Film Microstructure to Macroscopic Device Performance. *Chemistry of Materials* **2019,** *31* (17), 6530-6539.
13. Zhang, G.; McBride, M.; Persson, N.; Lee, S.; Dunn, T. J.; Toney, M. F.; Yuan, Z.; Kwon, Y.-H.; Chu, P.-H.; Risteen, B.; Reichmanis, E., Versatile Interpenetrating Polymer Network Approach to Robust Stretchable Electronic Devices. *Chemistry of Materials* **2017,** *29* (18), 7645-7652.
14. Park, B.; Kang, H.; Ha, Y. H.; Kim, J.; Lee, J.-H.; Yu, K.; Kwon, S.; Jang, S.-Y.; Kim, S.; Jeong, S.; Hong, S.; Byun, S.; Kwon, S.-K.; Kim, Y.-H.; Lee, K., Direct Observation of Confinement Effects of Semiconducting Polymers in Polymer Blend Electronic Systems. *Advanced Science* **2021,** *8* (14), 2100332.
15. Janasz, L.; Borkowski, M.; Blom, P. W. M.; Marszalek, T.; Pisula, W., Organic Semiconductor/Insulator Blends for Elastic Field-Effect Transistors and Sensors. *Advanced Functional Materials* **2022,** *32* (7), 2105456.
16. Brixi, S.; Dindault, C.; King, B.; Lamontagne, H. R.; Shuhendler, A. J.; Swaraj, S.; Lessard, B. H., Poly(2-vinylpyridine) as an Additive for Enhancing N-Type Organic Thin-Film Transistor Stability. *Advanced Electronic Materials* **2024,** *10* (2), 2300660.
17. Tran, H.; Feig, V. R.; Liu, K.; Wu, H.-C.; Chen, R.; Xu, J.; Deisseroth, K.; Bao, Z., Stretchable and Fully Degradable Semiconductors for Transient Electronics. *ACS Central Science* **2019,** *5* (11), 1884-1891.
18. Chua, L.-L.; Ho, P. K. H.; Sirringhaus, H.; Friend, R. H., Observation of Field-Effect Transistor Behavior at Self-Organized Interfaces. *Advanced Materials* **2004,** *16* (18), 1609-1615.
19. Kim, J.-S.; Ho, P. K. H.; Murphy, C. E.; Friend, R. H., Phase Separation in Polyfluorene-Based Conjugated Polymer Blends: Lateral and Vertical Analysis of Blend Spin-Cast Thin Films. *Macromolecules* **2004,** *37* (8), 2861-2871.
20. Nilsson, S.; Bernasik, A.; Budkowski, A.; Moons, E., Morphology and Phase Segregation of Spin-Casted Films of Polyfluorene/PCBM Blends. *Macromolecules* **2007,** *40* (23), 8291-8301.
21. Ren, F.; Ward, L.; Williams, T.; Laws, K. J.; Wolverton, C.; Hattrick-Simpers, J.; Mehta, A., Accelerated discovery of metallic glasses through iteration of machine learning and high-throughput experiments. *Science Advances* **2018,** *4* (4), eaaq1566.
22. Yin, X.; Yang, J.; Wang, H., Vertical Phase Separation Structure for High-Performance Organic Thin-Film Transistors: Mechanism, Optimization Strategy, and Large-Area Fabrication

toward Flexible and Stretchable Electronics. *Advanced Functional Materials* **2022,** *32* (27), 2202071.
23. Chang, M.; Lee, J.; Chu, P. H.; Choi, D.; Park, B.; Reichmanis, E., Anisotropic assembly of conjugated polymer nanocrystallites for enhanced charge transport. *ACS Appl Mater Interfaces* **2014,** *6* (23), 21541-9.
24. Gomez, I. J.; Wu, J.; Roper, J.; Beckham, H.; Meredith, J. C., High Throughput Screening of Mechanical Properties and Scratch Resistance of Tricomponent Polyurethane Coatings. *ACS Applied Polymer Materials* **2019,** *1* (11), 3064-3073.
25. Green, M. L.; Choi, C. L.; Hattrick-Simpers, J. R.; Joshi, A. M.; Takeuchi, I.; Barron, S. C.; Campo, E.; Chiang, T.; Empedocles, S.; Gregoire, J. M.; Kusne, A. G.; Martin, J.; Mehta, A.; Persson, K.; Trautt, Z.; Van Duren, J.; Zakutayev, A., Fulfilling the promise of the materials genome initiative with high-throughput experimental methodologies. *Applied Physics Reviews* **2017,** *4* (1), 011105.
26. Hoogenboom, R.; Meier, M. A. R.; Schubert, U. S., Combinatorial Methods, Automated Synthesis and High-Throughput Screening in Polymer Research: Past and Present. *Macromolecular Rapid Communications* **2003,** *24* (1), 15-32.
27. Kennedy, K.; Stefansky, T.; Davy, G.; Zackay, V. F.; Parker, E. R., Rapid Method for Determining Ternary-Alloy Phase Diagrams. *Journal of Applied Physics* **2004,** *36* (12), 3808-3810.
28. Meier, M. A. R.; Schubert, U. S., Combinatorial polymer research and high-throughput experimentation: powerful tools for the discovery and evaluation of new materials. *Journal of Materials Chemistry* **2004,** *14* (22), 3289-3299.
29. Meredith, J. C.; Smith, A. P.; Karim, A.; Amis, E. J., Combinatorial Materials Science for Polymer Thin-Film Dewetting. *Macromolecules* **2000,** *33* (26), 9747-9756.
30. Miracle, D. B.; Miller, J. D.; Senkov, O. N.; Woodward, C.; Uchic, M. D.; Tiley, J., Exploration and Development of High Entropy Alloys for Structural Applications. *Entropy* **2014,** *16* (1), 494-525.
31. Reetz, M. T., Combinatorial and Evolution-Based Methods in the Creation of Enantioselective Catalysts. *Angewandte Chemie International Edition* **2001,** *40* (2), 284-310.
32. Taniike, T.; Kitamura, T.; Nakayama, K.; Takimoto, K.; Aratani, N.; Wada, T.; Thakur, A.; Chammingkwan, P., Stabilizer Formulation Based on High-Throughput Chemiluminescence Imaging and Machine Learning. *ACS Applied Polymer Materials* **2020,** *2* (8), 3319-3326.
33. Xiang, X.-D.; Sun, X.; Briceño, G.; Lou, Y.; Wang, K.-A.; Chang, H.; Wallace-Freedman, W. G.; Chen, S.-W.; Schultz, P. G., A Combinatorial Approach to Materials Discovery. *Science* **1995,** *268* (5218), 1738-1740.
34. Alstrup, J.; Jørgensen, M.; Medford, A. J.; Krebs, F. C., Ultra Fast and Parsimonious Materials Screening for Polymer Solar Cells Using Differentially Pumped Slot-Die Coating. *ACS Applied Materials & Interfaces* **2010,** *2* (10), 2819-2827.
35. Genzer, J., Surface-Bound Gradients for Studies of Soft Materials Behavior. *Annual Review of Materials Research* **2012,** *42* (1), 435-468.
36. Liu, A. L.; Dogan-Guner, E. M.; McBride, M.; Venkatesh, R.; Gonzalez, M. A.; Reichmanis, E.; Grover, M.; Meredith, J. C., Composition Gradient High-Throughput Polymer Libraries Enabled by Passive Mixing and Elevated Temperature Operability. *Chemistry of Materials* **2022,** *34* (15), 6659-6670.

37. Meredith, J. C.; Karim, A.; Amis, E. J., High-Throughput Measurement of Polymer Blend Phase Behavior. *Macromolecules* **2000,** *33* (16), 5760-5762.
38. Rodríguez-Martínez, X.; Sevim, S.; Xu, X.; Franco, C.; Pamies-Puig, P.; Córcoles-Guija, L.; Rodriguez-Trujillo, R.; del Campo, F. J.; Rodriguez San Miguel, D.; deMello, A. J.; Pané, S.; Amabilino, D. B.; Inganäs, O.; Puigmartí-Luis, J.; Campoy-Quiles, M., Microfluidic-Assisted Blade Coating of Compositional Libraries for Combinatorial Applications: The Case of Organic Photovoltaics. *Advanced Energy Materials* **2020,** *10* (33), 2001308.
39. Harillo-Baños, A.; Rodríguez-Martínez, X.; Campoy-Quiles, M., Efficient Exploration of the Composition Space in Ternary Organic Solar Cells by Combining High-Throughput Material Libraries and Hyperspectral Imaging. *Advanced Energy Materials* **2020,** *10* (1), 1902417.
40. An, N. G.; Kim, J. Y.; Vak, D., Machine learning-assisted development of organic photovoltaics via high-throughput in situ formulation. *Energy & Environmental Science* **2021,** *14* (6), 3438-3446.
41. Eyke, N. S.; Koscher, B. A.; Jensen, K. F., Toward Machine Learning-Enhanced High-Throughput Experimentation. *Trends in Chemistry* **2021,** *3* (2), 120-132.
42. Rodríguez-Martínez, X.; Pascual-San-José, E.; Campoy-Quiles, M., Accelerating organic solar cell material's discovery: high-throughput screening and big data. *Energy Environ Sci* **2021,** *14* (6), 3301-3322.
43. Sun, S.; Hartono, N. T. P.; Ren, Z. D.; Oviedo, F.; Buscemi, A. M.; Layurova, M.; Chen, D. X.; Ogunfunmi, T.; Thapa, J.; Ramasamy, S.; Settens, C.; DeCost, B. L.; Kusne, A. G.; Liu, Z.; Tian, S. I. P.; Peters, I. M.; Correa-Baena, J.-P.; Buonassisi, T., Accelerated Development of Perovskite-Inspired Materials via High-Throughput Synthesis and Machine-Learning Diagnosis. *Joule* **2019,** *3* (6), 1437-1451.
44. Tran, V. V.; Jeong, G.; Kim, K. S.; Kim, J.; Jung, H.-R.; Park, B.; Park, J.-J.; Chang, M., Facile Strategy for Modulating the Nanoporous Structure of Ultrathin π-Conjugated Polymer Films for High-Performance Gas Sensors. *ACS Sensors* **2022,** *7* (1), 175-185.
45. Cascarini de Torre, L. E.; Flores, E. S.; Bottani, E. J., Nitrogen Physisorption on Modified Silica Surfaces. *Langmuir* **2000,** *16* (4), 1896-1901.
46. Ibach, H.; Horn, K.; Dorn, R.; Lüth, H., The adsorption of oxygen on silicon (111) surfaces. I. *Surface Science* **1973,** *38* (2), 433-454.
47. Campos, A.; Riera-Galindo, S.; Puigdollers, J.; Mas-Torrent, M., Reduction of Charge Traps and Stability Enhancement in Solution-Processed Organic Field-Effect Transistors Based on a Blended n-Type Semiconductor. *ACS Applied Materials & Interfaces* **2018,** *10* (18), 15952-15961.
48. Goffri, S.; Müller, C.; Stingelin-Stutzmann, N.; Breiby, D. W.; Radano, C. P.; Andreasen, J. W.; Thompson, R.; Janssen, R. A. J.; Nielsen, M. M.; Smith, P.; Sirringhaus, H., Multicomponent semiconducting polymer systems with low crystallization-induced percolation threshold. *Nature Materials* **2006,** *5* (12), 950-956.
49. Kang, J.; Shin, N.; Jang, D. Y.; Prabhu, V. M.; Yoon, D. Y., Structure and properties of small molecule-polymer blend semiconductors for organic thin film transistors. *Journal of the American Chemical Society* **2008,** *130* (37), 12273-12275.
50. Madec, M.-B.; Crouch, D.; Llorente, G. R.; Whittle, T. J.; Geoghegan, M.; Yeates, S. G., Organic field effect transistors from ambient solution processed low molar mass semiconductor–insulator blends. *Journal of Materials Chemistry* **2008,** *18* (27), 3230-3236.

51. Ohe, T.; Kuribayashi, M.; Tsuboi, A.; Satori, K.; Itabashi, M.; Nomoto, K., Organic Thin-Film Transistors with Phase Separation of Polymer-Blend Small-Molecule Semiconductors: Dependence on Molecular Weight and Types of Polymer. *Applied Physics Express* **2009,** *2* (12), 121502.
52. Xu, J.; Wang, S.; Wang, G. N.; Zhu, C.; Luo, S.; Jin, L.; Gu, X.; Chen, S.; Feig, V. R.; To, J. W.; Rondeau-Gagné, S.; Park, J.; Schroeder, B. C.; Lu, C.; Oh, J. Y.; Wang, Y.; Kim, Y. H.; Yan, H.; Sinclair, R.; Zhou, D.; Xue, G.; Murmann, B.; Linder, C.; Cai, W.; Tok, J. B.; Chung, J. W.; Bao, Z., Highly stretchable polymer semiconductor films through the nanoconfinement effect. *Science* **2017,** *355* (6320), 59-64.
53. Zhao, K.; Ding, Z.; Xue, L.; Han, Y., Crystallization-Induced Phase Segregation Based on Double-Crystalline Blends of Poly(3-hexylthiophene) and Poly(ethylene glycol)s. *Macromolecular Rapid Communications* **2010,** *31* (6), 532-538.
54. Lamport, Z. A.; Haneef, H. F.; Anand, S.; Waldrip, M.; Jurchescu, O. D., Tutorial: Organic field-effect transistors: Materials, structure and operation. *Journal of Applied Physics* **2018,** *124* (7).
55. Sirringhaus, H., Device Physics of Solution-Processed Organic Field-Effect Transistors. *Advanced Materials* **2005,** *17* (20), 2411-2425.
56. An, T. K.; Kang, I.; Yun, H. J.; Cha, H.; Hwang, J.; Park, S.; Kim, J.; Kim, Y. J.; Chung, D. S.; Kwon, S. K.; Kim, Y. H.; Park, C. E., Solvent additive to achieve highly ordered nanostructural semicrystalline DPP copolymers: toward a high charge carrier mobility. *Adv Mater* **2013,** *25* (48), 7003-9.
57. Kang, I.; Yun, H.-J.; Chung, D. S.; Kwon, S.-K.; Kim, Y.-H., Record High Hole Mobility in Polymer Semiconductors via Side-Chain Engineering. *Journal of the American Chemical Society* **2013,** *135* (40), 14896-14899.
58. Coveney, S., *Fundamentals of Phase Separation in Polymer Blend Thin Films*. 1 ed.; Springer Cham: 2015.
59. Snyder, H. L.; Meakin, P., Details of phase separation processes in polymer blends. *Journal of Polymer Science: Polymer Symposia* **1985,** *73* (1), 217-239.
60. Wei, P.; Li, X.; Wang, L.; Liu, N.; He, S.; Ren, Y.; Zhu, Y.; Yang, Y.; Lu, G.; Bu, L., Vertical-Resolved Composition and Aggregation Gradient of Conjugated-Polymer@Insulator-Matrix for Transistors and Memory. *Advanced Electronic Materials* **2020,** *6* (4), 1901156.
61. Gelles, R.; Frank, C. W., Effect of molecular weight on polymer blend phase separation kinetics. *Macromolecules* **1983,** *16* (9), 1448-1456.
62. Dobry, A.; Boyer-Kawenoki, F., Phase separation in polymer solution. *Journal of Polymer Science* **1947,** *2* (1), 90-100.
63. Lee, W. H.; Kwak, D.; Anthony, J. E.; Lee, H. S.; Choi, H. H.; Kim, D. H.; Lee, S. G.; Cho, K., The Influence of the Solvent Evaporation Rate on the Phase Separation and Electrical Performances of Soluble Acene-Polymer Blend Semiconductors. *Advanced Functional Materials* **2012,** *22* (2), 267-281.
64. Tipduangta, P.; Belton, P.; McAuley, W. J.; Qi, S., The use of polymer blends to improve stability and performance of electrospun solid dispersions: The role of miscibility and phase separation. *International Journal of Pharmaceutics* **2021,** *602*, 120637.
65. Müller-Buschbaum, P.; Gutmann, J. S.; Stamm, M., Influence of Blend Composition on Phase Separation and Dewetting of Thin Polymer Blend Films. *Macromolecules* **2000,** *33* (13), 4886-4895.

66. Park, H.; Yoo, S.; Won, J. C.; Kim, Y. H., Room-temperature, printed, low-voltage, flexible organic field-effect transistors using soluble polyimide gate dielectrics. *APL Materials* **2020,** *8* (1), 011112.
67. Callaway, C. P.; Liu, A. L.; Venkatesh, R.; Zheng, Y.; Lee, M.; Meredith, J. C.; Grover, M.; Risko, C.; Reichmanis, E., The Solution is the Solution: Data-Driven Elucidation of Solution-to-Device Feature Transfer for π-Conjugated Polymer Semiconductors. *ACS Applied Materials & Interfaces* **2022,** *14* (3), 3613-3620.
68. Chang, M.; Lee, J.; Kleinhenz, N.; Fu, B.; Reichmanis, E., Photoinduced Anisotropic Supramolecular Assembly and Enhanced Charge Transport of Poly(3-hexylthiophene) Thin Films. *Advanced Functional Materials* **2014,** *24* (28), 4457-4465.
69. Park, S. Y.; Kwon, E. H.; Park, Y. D., Effect of localized UV irradiation on the crystallinity and electrical properties of dip-coated polythiophene thin films. *RSC Advances* **2020,** *10* (56), 34130-34136.
70. Wang, G.; Persson, N.; Chu, P.-H.; Kleinhenz, N.; Fu, B.; Chang, M.; Deb, N.; Mao, Y.; Wang, H.; Grover, M. A.; Reichmanis, E., Microfluidic Crystal Engineering of π-Conjugated Polymers. *ACS Nano* **2015,** *9* (8), 8220-8230.
71. Chang, M.; Su, Z.; Egap, E., Alignment and Charge Transport of One-Dimensional Conjugated Polymer Nanowires in Insulating Polymer Blends. *Macromolecules* **2016,** *49* (24), 9449-9456.
72. Xu, Z.; Park, K. S.; Diao, Y., What Is the Assembly Pathway of a Conjugated Polymer From Solution to Thin Films? *Frontiers in Chemistry* **2020,** *8*.
73. Park, K. S.; Kwok, J. J.; Dilmurat, R.; Qu, G.; Kafle, P.; Luo, X.; Jung, S.-H.; Olivier, Y.; Lee, J.-K.; Mei, J.; Beljonne, D.; Diao, Y., Tuning conformation, assembly, and charge transport properties of conjugated polymers by printing flow. *Science Advances 5* (8), eaaw7757.
74. Qu, G.; Zhao, X.; Newbloom, G. M.; Zhang, F.; Mohammadi, E.; Strzalka, J. W.; Pozzo, L. D.; Mei, J.; Diao, Y., Understanding Interfacial Alignment in Solution Coated Conjugated Polymer Thin Films. *ACS Applied Materials & Interfaces* **2017,** *9* (33), 27863-27874.
75. Afzal, T.; Iqbal, M. J.; Iqbal, M. Z.; Sajjad, A.; Raza, M. A.; Riaz, S.; Kamran, M. A.; Numan, A.; Naseem, S., Effect of post-deposition annealing temperature on the charge carrier mobility and morphology of DPPDTT based organic field effect transistors. *Chemical Physics Letters* **2020,** *750*, 137507.
76. Chen, Z.; Lee, M. J.; Shahid Ashraf, R.; Gu, Y.; Albert-Seifried, S.; Meedom Nielsen, M.; Schroeder, B.; Anthopoulos, T. D.; Heeney, M.; McCulloch, I.; Sirringhaus, H., High-performance ambipolar diketopyrrolopyrrole-thieno[3,2-b]thiophene copolymer field-effect transistors with balanced hole and electron mobilities. *Adv Mater* **2012,** *24* (5), 647-52.
77. Park, H.; Yoo, S.; Won, J. C.; Kim, Y. H., Room-temperature, printed, low-voltage, flexible organic field-effect transistors using soluble polyimide gate dielectrics. *APL Materials* **2020,** *8* (1), 011112.

Table of Contents Graphic (TOC)